AD-A177 937 SATELLITE OBSERVATION OF ATMOSPHERIC NUCLEAR GAMMA RADIATION(U) SEVERN COMMUNICATIONS CORP SEVERNA PARK MD J R LETAW ET AL. JAN 87 N00014-85-C-2200 1/1

UNCLASSIFIED F/G 18/8 NL

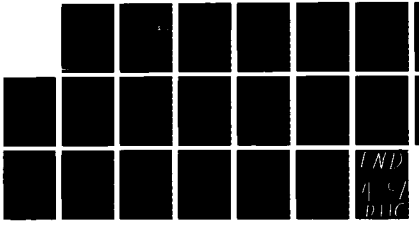

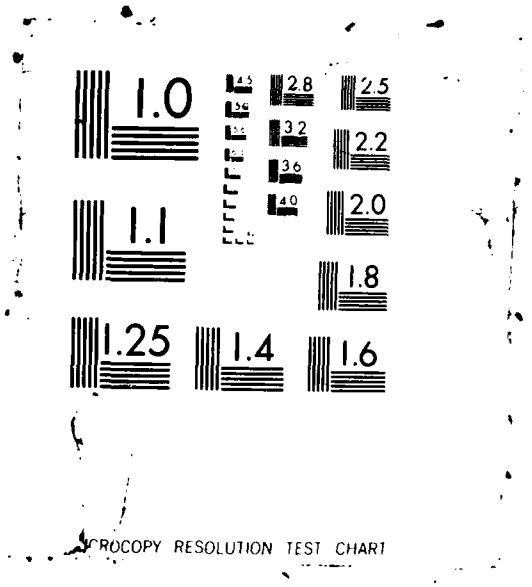
1.0
1.1
1.25
1.4
1.6
1.8
2.0
2.2
2.5
2.8
3.2
3.6
4.0
ROCOPY RESOLUTION TEST CHART

Contract N00014-85-C-2200
Severn Communications Corporation
Severna Park, MD 21146

SATELLITE OBSERVATION OF ATMOSPHERIC NUCLEAR GAMMA RADIATION

J.R. Letaw
Severn Communications Corporation

G.H. Share, R.L. Kinzer, R. Silberberg, and C.H. Tsao
E.O. Hulburt Center for Space Research
Naval Research Laboratory

E.L. Chupp and D.J. Forrest
Physics Department
University of New Hampshire

E. Rieger
Max Planck Institut fur Physik und Astrophysik

ABSTRACT

We present a satellite observation of the spectrum of gamma radiation from the Earth's atmosphere in the energy interval from 300 keV to 8.5 MeV. The data were accumulated by the Gamma Ray Spectrometer on the Solar Maximum Mission over three and one-half years. The excellent statistical accuracy of the data set allows 20 atmospheric line features to be distinguished. All observed lines are consistent with production by secondary neutron interactions with atmospheric ^{14}N and ^{16}O. Although, we find no evidence for other production mechanisms, we cannot rule out direct excitation or spallation by primary protons as a source of atmospheric line radiation. Line intensities are in rough agreement with theoretical models which are presently limited by cross section availability. The intensity and spectrum of scattered photons at energies below the 0.511 MeV line can be accounted for by Compton scattering in a 21 g/cm^2 slab of atmosphere.

INTRODUCTION

Among astrophysical sources of gamma radiation, the Earth is by far the most intense object observed by satellite-borne spectrometers. Cosmic radiation traversing the upper atmosphere is responsible for a complex series of interactions ultimately leading to a gamma ray albedo. This radiation is generally a nuisance to satellite and balloon-borne gamma-ray telescopes. An understanding of atmospheric gamma radiation as a source of background may enhance the observations of future satellite-borne detectors such as the spectrometers on the Gamma Ray Observatory. In addition, the intense and complex line structure offers the potential of in-flight detector calibration.

The atmospheric gamma ray spectrum contains a a wealth of detail on neutron and proton-induced gamma-ray lines in a complex medium. Most critical factors, such as molecular composition of the atmosphere, irradiation levels, and geometry are well known and allow for extensive tests of our understanding of complex transport processes. Improvements in our knowledge of less well-known transport factors, such as neutron cross sections, are also possible. Measurements to the precision allowed by existing detectors therefore offer an ideal environment for testing models of gamma ray emissions from the planets, the sun, and other astrophysical sources.

In this paper we present observations and analysis of the atmospheric gamma ray albedo in the range from 0.3 to 8.5 MeV. The data were collected by the gamma ray spectrometer on the Solar Maximum Mission (SMM) satellite over the period February, 1980 through September, 1983. The spectrometer always points at the Sun and therefore views the Earth during approximately half of its orbit. Data accumulated over 1.5×10^6 seconds of detector live time and having unprecedented statistical significance has been obtained. The raw spectrum consists of lines of atmospheric origin and lines intrinsic to the detector, all superimposed on a continuum background. Our analysis of this data set reveals 20 atmospheric gamma ray lines (at varying levels of significance), most of which have not been observed before.

The atmospheric gamma ray spectrum has been observed previously on several occasions. Peterson, Schwartz, and Ling (1973) have reported a ballon measurement of the atmospheric background spectrum below 10 MeV. They show clearly the 0.511 MeV line, which is presumably due to annihilation of positrons produced in air showers. The remainder of the spectrum (above 1 MeV) is described as a "steep and relatively structureless continuum." The continuum was represented as a power law with spectral index -1.4. Ryan et al. (1977) and Lockwood et al. (1979) report measurements of the upward moving gamma ray background in the

range 2 to 20 MeV. Their observed count rate spectral indices are consistent with Peterson, Schwartz, and Ling's isotropic measurement.

Groups from the Naval Research Laboratory and Goddard Space Flight Center (Ling 1975) privately communicated measurements of the 2.31 MeV line from 14N, the 4.44 MeV line from 12C and 11B, the 6.1MeV line from 16O, and the line complex at about 6.7 MeV. Willett et al. (1979) have made a further report of the 6.13 MeV line. Numerous observations of the positron decay line at 0.511 MeV have been reported (Mahoney, Ling, and Jacobsen, 1981 and references therein). **Possible additional reference by Dunfie and Chupp**

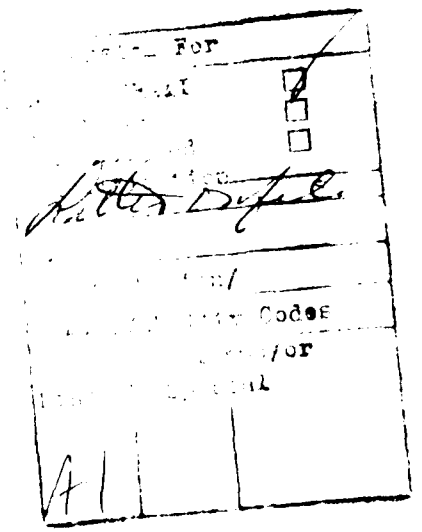

INSTRUMENT

NASA's Solar Maximum Mission Satellite (SMM) was launched on February 14, 1980. The gamma-ray spectrometer (GRS) is one of seven instruments designed to study the Sun over a broad spectral range from the visual to energies in excess of 10 MeV. It consists of seven cylindrical 7.5 cm x 7.5 cm NaI scintillation detectors, shielded by a 2.5 cm thick CsI annulus and a 7.6 cm CsI back plate which defines a broad aperture of $\approx 130^{o}$ FWHM (Forrest et al., 1980). The 7 detectors are actively gain stabilized; their outputs are summed to register the total energy loss of gamma-ray events unaccompanied by a signal indicating an interaction in the CsI shields or plastic scintillation detectors, which complete the 4<pi> anticoincidence shield for charged particles. Spectra are accumulated each 16.38 s.

The active gain control has performed flawlessly and permits spectra accumulated over tens of months to be summed without degradation in resolution (7% FWHM at 662 keV). This capability has made possible the detection of the interstellar ^{26}Al line (Share et al. 1985). As we discuss below, it also allows atmospheric lines to be measured with unprecedented statistical significance.

DATA SET AND ANALYSIS

The data set analyzed in this paper was collected over the period February, 1980 through September, 1983. The observed count spectrum (Figure 1) consists of data accumulated while the center of the Earth was within 36^{o} of the detector axis and when the vertical rigidity cutoff was less than 11 GV. Under these conditions the relative intensity of the atmospheric lines is greatest. To reduce instrumental background from trapped protons, the data set is restricted to periods more than 10^{4} s after the last significant South Atlantic Anomaly passage.

The observed count spectrum contains intrinsic detector lines, background from radioactivity in the spacecraft induced by energetic particle interactions, and gamma radiation emitted from the atmosphere. ^{60}Co lines at 1.17 MeV and 1.33 MeV are leakage from a gain stabilization source within the detector. Other lines from the decay of spallation products of sodium, iodine, cesium, iron, and nickel within the instrument are also visible. Atmospheric lines at 0.511 MeV and 4.44 MeV (from ^{11}B or ^{12}C) stand out in the count spectrum. They are the strongest features of atmospheric origin.

Instrumental background is reduced by subtracting a count spectrum accumulated under the same conditions as the original count spectrum, except that the detector is pointing at an angle of 144^{o} or more away from the Earth. As shown in Figure 2 the ^{60}Co calibration lines and other internal background features are essentially eliminated by this procedure. Residual intensities of background lines are about 1% of their intensity in the raw count spectrum.

Details of the observed count spectrum is shown in Figures 3 through 7. Strong features of the spectrum appear at 0.511 MeV, 4.45 MeV, and 6.18 MeV. Much additional structure is also visible. The statistical significance of the data set is excellent as indicated by plotted uncertainties. About 10^{8} atmospheric photons are accumulated in the spectrum. Limiting errors in the analysis which follows are systematic.

Analysis of this data set is characterized by the difficulty of determining the energy, intensity, and width of the many overlapping lines evident in the figures. There is a substantial amount of information in the spectrum and several data analysis steps are required to extract it. First, the continuum background is estimated. Then line features are identified and their approximate intensities found. A non-linear curve fitting program is used to fix the line characteristics precisely. Finally, manual modifications to reduce the overall $\langle chi \rangle^{2}$/DOF are introduced.

Each data analysis step begins with a model of the photon spectrum incident on the detector. This model is composed of a power-law continuum with an arbitrary number of Gaussian lines superimposed. It is then folded through an instrument respose matrix to produce the expected count spectrum. The response matrix has been derived from detector calibrations and Monte Carlo simulations, and has been applied successfully to the analysis of solar gamma-ray spectra (Murphy, 1985). The detector reponse matrix contains channel energy and width assignments, accounts for Compton scattering and escape peaks, and corrections for detector non-linearities. Comparison of the expected count spectrum within the detector with the observed spectrum is facilitated by the $\langle chi \rangle^2$ test.

The structure of our model imposes some limitations on the observational results. The restriction to Gaussian-shaped lines is not strictly correct. Line blending and Doppler shifts are expected to cause varied line shapes. No attempt has been made to decompose strongly blended lines into individual constituents or to model the structure of Doppler shifted lines. Both efforts depend critically on our currently inadequate understanding of line production mechanisms within the atmosphere. Furthermore a power-law may only approximate the atmospheric continuum. Deviations from a pure power law will be reflected as systematic errors in line shape parameters.

The underlying power law continuum is established by fitting to data in the ranges 0.9 to 1.0 MeV and 7.5 to 8.5 MeV where strong atmospheric line features are neither observed nor expected. The exact parameters of this continuum spectrum are allowed to vary in later fitting steps. The final power law index (exponent of dN/dE) of the atmospheric photon spectrum is -1.16. This translates into an observed count spectrum index (within the detector) of -1.63.

The count spectrum index (-1.63) is presented for comparison with previous measurements. It is somewhat steeper than reported by Peterson et al. (1973) who measured a value of -1.4. We believe the difference exists because line features above 1 MeV were not resolved by their instrument and, hence, were incorporated into the continuum. This causes the observed continuum to appear flatter.

While the model fit to data is visually appealing, the overall $\langle chi \rangle^2$/DOF for the fit over the interval 1.5 MeV to 8.5 MeV is 2.4. $\langle chi \rangle^2$/DOF is even less satisfactory at lower energies as described in the discussion below. We have been unable to improve the fit within the confines of our spectrum and detector models. Possible reasons for this are:

(1) Line feature shapes are not always well approximated by Gaussians. These shapes are determined by blending of multiple lines and by reaction kinematics, neither of which is included in this analysis.

(2) Statistics are so good within this data set that changes in the number of counts from bin to bin are often much greater than the statistical uncertainty in a given bin. In this case, the midpoint of the bin is not a good approximation to the mean energy deposited by a photon appearing in that bin. This problem is at its worst at low energies where statistics are best. (For example, our best fit to the 0.511 MeV line discussed below has $\langle chi \rangle^2$/DOF of about 60.)

(3) Our knowledge of detector reponse, as represented in the detector model, is founded on calibrations involving fewer photons than the atmospheric data set. Residual uncertainty in the detector model may contribute to an increased $\langle chi \rangle^2$/DOF. Variations of 2 or 3 standard deviations in the number of counts from one channel to the next are common. Such features should not exist in a spectrum where lines are broadened. $\langle chi \rangle^2$/DOF over the interval 1.5 MeV to 8.5 MeV for a smoothed data set, in which the number of counts in each channel is averaged with its two neighbors, is 1.0. This suggests that assignment of individual channel widths may be in error by a few percent. This differential non-linearity is not significant in other SMM data sets.

DISCUSSION

a) Line Intensities

The intensities of gamma ray lines from the atmosphere were predicted by Ling (1975) using a semiempirical model. The model assumes that gamma ray lines (other than 0.511 MeV) result from neutron absorption and inelastic scattering reactions on ^{14}N and ^{16}O. A source function at zero depth is defined as the rate of gamma ray production in a medium of atmospheric composition by a spectrum of neutrons with the shape of the atmospheric neutron spectrum. It relies on cross sections for gamma ray production in neutron interactions and is taken to be isotropic. The source function at arbitrary atmospheric depth is modeled using a measured neutron growth curve. Integration of the source function over the atmosphere and accounting for attenuation yields the angle-dependent gamma ray line intensity. Ling's model does not predict the widths of atmospheric gamma ray lines.

Figure 8 shows a comparison of our results with Ling's predictions where comparison is possible. Ling provides upper and lower limits of line intensities (shown as boxes in the Figure) which typically differ by an order of magnitude. The absence of neutron cross sections above 17 MeV prevented a more precise determination of the intensity. The height of each box spans the measured FWHM of line features within the energy range which were summed to compare with Ling's predictions. Reasonable agreement is found within the broad limits of this comparison except in one case. The feature at 3.03 MeV is more than an order of magnitude more intense than expected by Ling. This discrepancy is discussed later in this section.

Heavy vertical lines in Figure 8 are estimates of the atmospheric gamma ray line intensities derived from Reedy's (1978) calculation of lunar gamma ray line intensities. Lunar soil is composed primarily of oxygen, but contains some nitrogen. Relative atmospheric gamma ray line intensities may therefore be derived from Reedy's tables by adjusting for the difference in composition. Reedy adopted a neutron spectrum having the same shape as the atmospheric neutron spectrum and estimated the high energy (> 17 MeV) neutron cross sections. This modified version of Reedy's calculations is also in reasonable agreement with our measurements except for the feature at 3.03 MeV.

(b) Line Widths

As seen in Figures 3 - 7, the observed atmospheric gamma ray line features have widely varying widths. There are several possible causes for this line broadening:

(1) Instrumental broadening due to the relatively poor energy resolution of the NaI detector.

(2) Doppler broadening of the line due to nuclear recoil momentum at the time of deexcitation.

(3) Blending of multiple lines which are not resolved by the detector.

The first possible cause is eliminated by the instrumental model incorporated into our analysis procedures. An energy-dependent instrumental width (approximately 30 keV (FWHM) at 1 MeV) has been accounted for in our reported widths. The instrumental width obscures the actual widths of some narrow line features.

Doppler broadening occurs in atmospheric lines when, after a nuclear reaction, a nuclide undergoes the gamma-ray-emitting transition before ionization losses stop it. The mean pathlength traveled before decay is:

$$\langle\lambda\rangle = \langle\rho\rangle v \langle\bar{\tau}\rangle$$

where $\langle\rho\rangle$ is atmospheric density at the altitude where the reaction occurs, v is the recoil velocity, and $\langle\bar{\tau}\rangle$ is the mean lifetime of the excited state. (Time dilation is negligible.)

An upper limit on transition pathlength in the upper atmosphere may be calculated. Assume $\langle\rho\rangle$ is atmospheric density at sea level (about 50 times greater than at 20 g/cm^2). Assume the mean lifetime of a level is 100 ps (which exceeds the lifetime of the 6.049 level of ^{16}O, the longest-lived state of interest to us). Finally, assume v = .2c corresponding to a higher than average recoil energy of 20 MeV. The upper limit on pathlength is then

$$\langle\lambda\rangle << 10^{-4} \text{ g/cm}^2 \quad .$$

This upper limit on level decay pathlength is substantially smaller than the typical range of a recoil product (about 10^{-3} g/cm^2).

We conclude from the discussion above that all lines will suffer the maximum amount of Doppler broadening. While consequently some intrinsic width in the lines is expected from Doppler broadening, wide variations in width are not. For example, the line feature at 5.12 MeV (presumably from the 8.6 ps transition to ground state of ^{14}N) has a width of 550 keV (FWHM), but the line feature at 2.32 MeV (presumably from the 0.06 ps transition to ground state of ^{14}N) has a width of only 80 keV (FWHM). Doppler broadening cannot account for this difference; if anything, it would cause a variation in the reverse direction.

It is likely that line blending is the predominant cause of the observed widths of the atmospheric gamma ray line features. Gamma ray lines observed in nuclear reactions of light nuclei nave been tabulated by De Meijer et al. (1974) and are summarized in Table 2. (We have added two lines from transitions out of the 11.06 MeV state in ^{16}O which were mentioned by Ling.) About half of these lines are strong enough that they were included in Ling's (1975) modeling of neutron-induced reactions in the atmosphere and/or Murphy's (1985) modeling of proton-induced reactions in solar flares (Ramaty, Kozlovsky, and Lingenfelter, 1979). The reaction cross sections leading to most of these gamma rays are unknown. In general, more than one significant transition is contributing to each line feature identified in our analysis.

(c) Individual Line Features

A discussion of individual line features within each energy interval follows:

(0.4 MeV - 0.6 MeV)

The 0.511 MeV feature is narrow, and obscured by the instrumental width, and about 10 times more intense than the strongest nuclear line at 4.450 MeV. The Gaussian fit is not adequate below the peak because of Compton scattering in the atmosphere. The fit is much improved by introducing a 21 ± 1 g/cm^2 slab of atmosphere between the Gaussian source line and the detector. The $\langle chi \rangle^2$/DOF measure of fit (about 50) is not useful in this interval because of the large bin widths and excellent statistical accuracy of the data.

A line feature is required at 0.64 MeV when Compton scattering is not included in the fit. This feature compensates for scattered radiation from the feature observed at 0.74 MeV.

(0.7 MeV - 0.8 MeV) $\langle chi \rangle^2/DOF = 3.9$

This relatively narrow feature is well fit by a line at 0.735 MeV. Ling predicts a line from the ^{14}N transition from 5.833 MeV to 5.106 MeV at nearly this energy. $\langle chi \rangle^2$ suffers from the excellent statistical accuracy of the data.

(0.8 MeV - 1.5 MeV)

No lines of atmospheric origin were identified in this interval. Residuals of the ^{60}Co calibration lines at 1.333 MeV and 1.165 MeV were fitted with negative intensities of -0.77 and -0.36 respectively (not shown in Figure 4). These lines are approximately 1% of their intensity in the raw spectrum; a measure of t accuracy of the "down minus up" subtraction. Other background lines from the detector and detector superstructure which have not been subtracted

completely may appear in this interval, including direct excitation and spallation lines from Na, I, Cs, and Fe.

(1.5 MeV - 1.8 MeV) $\langle chi \rangle^2/DOF = 3.3$

The spectrum in this interval is fit by a single line at 1.63 MeV with 65 keV (FWHM). This relatively narrow feature results from a transition of ^{14}N from 3.945 to 2.313 MeV. $\langle chi \rangle^2/DOF$ is probably affected by the wide count bins in this region.

(1.8 MeV - 2.2 MeV) $\langle chi \rangle^2/DOF = 1.6$

A strong line feature is observed in this interval at 2.14 MeV. A line from ^{11}B at the measured intensity is expected at 2.124 MeV by Ling and by the modified calculation of Reedy. This feature is somewhat broader than the related line at 4.450 MeV. The line breadth may indicate a weak contribution from other transitions, such as at 2.190 from ^{16}O.

The weak feature at 1.90 MeV was inserted manually to make up a slight deficiency in counts. It may be due to the ^{11}C transition at 1.995 MeV.

(2.2 MeV - 2.4 MeV) $\langle chi \rangle^2/DOF = 1.1$

This relatively narrow feature is well-fitted by a Gaussian centered at 2.32 MeV. It is within 1.3 standard deviations of the expected ^{14}N line at 2.313 MeV and within a factor of two of Ling's predicted intensity.

(2.4 MeV - 2.9 MeV) $\langle chi \rangle^2/DOF = 1.3$

The fitted feature at 2.78 MeV has nearly the central energy and relative intensity predicted by Ling to come from the ^{16}O transition (8.872 MeV - 6.131 MeV). The feature has a 230 keV FWHM.

A feature at 2.54 MeV was inserted manually to make up a deficiency of counts in the region. Possible transitions at this energy are indicated in Table 2.

(2.9 MeV - 3.2 MeV) $\langle chi \rangle^2/DOF = 2.5$

There is only weak visual indication of a count enhancement in this interval. It is fit by a broad feature centered at 3.03 MeV. Ling predicts a ^{13}C line (from a ^{16}O reaction) in the interval. The feature is broad and may be a line blend; however, there are no strong candidates for additional lines (we have no evidence of any lines from ^{10}B or ^{10}Be). This feature is more than a factor of 10 stronger than predicted

by Ling which may result from neglect of the ^{13}C line from spallation of ^{14}N. It is also possible that our atmospheric continuum estimate is somewhat low in the vicinity of this line.

(3.2 MeV - 3.5 MeV) $\langle chi \rangle^2/DOF = 0.9$

This feature is fit by a broad line at 3.40 MeV. The 270 keV (FWHM) of this feature suggests a blend of several atmospheric lines. Ling predicts a single line from ^{14}N in this energy interval at no more than half the measured intensity. Candidates for other lines are shown in Table 2. An underestimate of the atmospheric continuum in this interval may also account for the excess.

(3.5 MeV - 3.8 MeV) $\langle chi \rangle^2/DOF = 1.5$

An excellent fit to a feature of moderate width (140 keV FWHM) is found in this interval at 3.69 MeV. A line from ^{13}C is expected in this energy inteval.

(3.8 MeV - 4.0 MeV) $\langle chi \rangle^2/DOF = 1.0$

An excellent fit to a feature of moderate width (150 keV FWHM) is found in this interval at 3.91 MeV. Lines from ^{13}C and ^{14}N of about equal strength are expected in this interval. The uncertainty in line intensities between 2 and 4 MeV is somewhat larger than at higher energies because of overlap in the detector response (broad features and escape peaks).

(4.0 MeV - 4.3 MeV) $\langle chi \rangle^2/DOF = 4.4$

A weak feature at 4.19 MeV was required by the fitting routine to fill in the energy interval between 4 and 4.3 MeV. There is marginal visual indication of a peak. The width of this feature could not be determined. Ling expects a weak feature from the decay of the 11.06 MeV level of ^{16}O at 4.140 MeV.

(4.3 MeV - 4.6 MeV) $\langle chi \rangle^2/DOF = 4.6$

The feature at 4.45 MeV is the strongest nuclear line feature from the atmosphere. Ling attributes it to the transition of the first excited state of ^{11}B to ground state yielding a line at 4.443 MeV. The mirror nucleus, ^{12}C, yields a line at 4.438 MeV and could also be contributing to the line intensity in this region. Both nuclides can be produced in neutron and proton spallation reactions with ^{14}N. The line width is about twice that of the narrow feature at 2.32 MeV; possibly because the excited spallation product has greater

recoil energy than a directly excited nucleus. We believe <chi>2 is large because the statistical uncertainty is low as has been discussed above.

(4.6 MeV - 5.4 MeV) $\langle chi \rangle^2/DOF = 3.3$

The feature at 5.12 MeV is the second strongest nuclear line feature from the atmosphere. Ling attributes this line almost entirely to the 5.105 MeV transition of ^{14}N to the ground state. This transition is the strongest line on his list, behind lines at 1.632 MeV and 2.313 MeV from ^{14}N as well as the strong line at 6.129 MeV. The width of this feature is 550 keV (FWHM) and by far the greatest among the features we have identified. It appears likely that other lines, possibly from the two lowest levels of ^{15}O and ^{15}N to the ground state, are contributing.

(5.4 MeV - 5.9 MeV) $\langle chi \rangle^2/DOF = 3.0$

The feature in this interval was poorly represented by a single Gaussian. We have fit it using two Gaussians centered at the expected ^{14}N gamma rays at 5.832 MeV and 5.690 MeV. The lines overlap strongly. This overlap introduces uncertainty into the line intensity and, in concert with instrumental broadening, obscures the width. The energy of the 5.611 MeV line is several standard deviations lower than expected and may indicate a contribution from ^{11}C at 5.513 MeV.

(5.9 - 6.3 MeV) $\langle chi \rangle^2/DOF = 1.7$

The spectrum in this region is well approximated by a Gaussian-shaped line centered at 6.178 $\pm$ 0.006 MeV with width 220 keV FWHM. While it is expected that the feature would be dominated by the 6.129 MeV line from ^{16}O, the energy is almost exactly equal to the 6.176 MeV line from ^{15}O. This could indicate contributions from other transitions listed in Table 2. It is of interest that a line feature centered at this energy is often observed by SMM in solar flares (ref.....). The feature width suggests that multiple lines are contributing. This feature is the third strongest nuclear line from the atmosphere.

(6.3 - 6.6 MeV) $\langle chi \rangle^2/DOF = 3.1$

The feature in this interval has been modeled with a single Gaussian centered at 6.46 MeV. This feature is relatively weak. While the fit approximates the line intensity well, the shape is not correctly represented as a Gaussian. Lines at 6.322 MeV from ^{15}N and at 6.442 MeV from ^{14}N are expected to occur in this interval. Two lines from ^{11}C may be present.

(6.6 - 7.2 MeV) $\langle chi \rangle^2/DOF = 1.6$

The spectrum is well approximated in this interval by a Gaussian centered at 6.927 $\pm$ 0.009 MeV. $\langle chi \rangle^2/DOF$ in this range is considerably smaller than obtained over the entire spectrum. The feature is broadened substantially more than 1% or 2% FWHM as expected in direct reactions of this sort (Murphy, 1985). Ling predicts that four lines of roughly equal strength from ^{16}O, ^{14}N, and ^{14}C contribute in this region.

(7.2 - 8.5 MeV) $\langle chi \rangle^2/DOF = 2.6$

The fit was not improved by introducing lines in this region. Any perceived features do not occur at physically meaningful energies corresponding to transitions of ^{15}N, ^{11}B, and ^{11}C.

CONCLUSION

In this paper we have presented an analysis of observed atmospheric gamma ray line features from 300 keV to 8.5 MeV. 20 features, of varying significance, were identified and assigned central energies, widths, and intensities. The spectral characteristics were assigned within a model based on a power-law spectrum continuum with Gaussian lines superimposed. These were compared with actual count data using a detector model.

The power-law continuum background was found to have an index of -1.16. The precise nature of the continuum is obscured by many superimposed lines. Our data suggests the proposed continuum may be slightly low in the region from 2.5 MeV to 3.5 MeV. In this region, the widths of the three line features (2.778,3.027,3.402) are somewhat greater than expected from reaction kinematics. From consideration of Table 2, it is likely that only a single line contributes to each feature. In addition, the line intensities are slightly greater than predicted by Ling (1975) (see Figure 8). Finally, a feature was added manually at 2.54 MeV, primarily because of a photon deficiency in that region. We have not attempted to refine our estimate of the background spectrum.

Our data leave the question of the origin of atmospheric gamma ray lines unanswered. The four most likely possibilities are:

1) Primary cosmic ray proton spallation and direct excitation reactions.

2) Spallation and direct excitation reactions of secondary neutrons produced by cosmic ray interactions in the atmosphere.

3) Spallation and direct excitation reactions of secondary protons produced by cosmic ray interactions in the atmosphere.

4) Absorption of secondary neutrons.

We believe (3) and (4) above are ruled out by our data and theoretical calculations. Ling (1975) shows that neutron absorption line in the atmosphere are one to two orders of magnitude less intense than the strongest atmospheric lines. We identify no features which can be attributed mainly to neutron absorption. Secondary protons are produced in roughly equal numbers to secondary neutrons, but because they have relatively little energy, they are unlikely to interact before stopping from ionization losses. For this reason, secondary neutrons are likely to dominate secondary protons as the cause of atmospheric gamma ray lines.

Spallation reactions of atmospheric constituents with cosmic ray protons are likely to result in ^{12}C. The line from ^{12}C at 4.438 MeV is indistinguishable from the prominent neutron scattering line $^{14}N(n,<alpha>)^{11}B^{*}$(4.444 MeV - g.s.) in our data set. In fact, similar spallation products are expected from cosmic ray protons and secondary neutrons. No distinct signature of cosmic ray primary interactions is found in our data; on the other hand, we cannot rule out a significant contribution from this source. Future theoretical analysis of these data may be allow separate contributions to be distinguished.

ACKNOWLEDGEMENTS

We appreciate discussions with Ron Murphy and Jim Ling on topics closely related to this research. The work of (J.P.L.) was supported in part by Naval Research Laboratory contract N00014-85-C-2200.

REFERENCES

De Meijer, R.J., Plendl, H.S., and Holub, R., Tables for Reaction Gamma-Ray Spectroscopy, Part I: A=6 to A=20, Atomic Data and Nuclear Data Tables, 13, 1-33, 1974.

DUNFY AND CHUBB ....

Forrest, D.J. et al., The Gamma Ray Spectrometer for the Solar Maximum Mission, Solar Phys., 65, 15-23, 1980.

Lederer, C.M. and Shirley, V.S., Table of Isotopes, J. Wiley and Sons, New York, 1978.

Ling, J.C., A Semiempirical Model for Atmospheric Gamma Rays from 0.3 to 10 MeV at 40° Geomagnetic Latitude, J. Geophys. Res., 80, 3241-3252, 1975.

Lockwood, J.A., Hsieh, L., Frilling, L., Chen, C., and Swartz, D., Atmospheric Neutron and Gamma Ray Fluxes and Energy Spectra, J. Geophys. Res., 84, 1402-1408, 1979.

Mahoney, W.A., Ling, J.C., and Jacobson, A.S., HEAO-3 Measurements of the Atmospheric Positron Annihilation Line, J. Geophys. Res., 86, 11098-11104, 1981.

Murphy, R., Gamma Rays and Neutrons from Solar Flares, Ph.D. Dissertation, NASA/Goddard Space Flight Center, 1985.

Peterson, L.E., Schwartz, D.A., and Ling, J.C., Spectrum of Atmospheric Gamma Rays to 10 MeV at Lambda = 40°, J. Geophys. Res., 78, 7942-7958, 1973.

Ramaty, R., Kozlovsky, B., and Lingenfelter, R.E., Nuclear Gamma-Rays from Energetic Particle Interactions, Ap. J. Suppl., 40, 487-526, 1979.

Reedy, R.C., Planetary Gamma Ray Spectroscopy, in: Gamma Ray Spectroscopy in Astrophysics, ed. T.L. Cline and R. Ramaty, NASA Technical Memorandum 79619, 1978.

Ryan,J.M, Dayton, B., Moon, S.H., Wilson, R.B., Zych, A.D., and White, S.R., Atmospheric Angle and Energy Distributions from 2 to 25 MeV, J. Geophys. Res., 82, 3593-3601, 1977.

Share, ...

Willett, J.B., Ling, J.C., Mahoney, W.A., and Jacobson, A.S., Detection of 6.13 MeV Gamma Rays Within and at the Top of the Atmosphere, Ap. J., 234, 753-760, 1979.

Table 1: Observed Atmospheric Gamma Ray Line Features
(Model Fit Parameters)

Energy (MeV)	Relative* Intensity	Width (keV FWHM)
6.927 ± .009	2.65 ± .09	400 ± 25
6.465 ± .016	0.87 ± .10	160 ± 30
6.178 ± .006	3.28 ± .11	220 ± 15
5.848 ± .018	0.57 ± .10	----
5.611 ± .011	0.69 ± .11	----
5.124 ± .008	4.17 ± .09	550 ± 25
4.450 ± .002	5.87 ± .09	180 ± 10
4.190 ± .020	0.75 ± .08	----
3.909 ± .024	1.73 ± .48	150 ± 60
3.693 ± .018	1.83 ± .63	140 ± 70
3.402 ± .024	1.51 ± .34	270 ± 80
3.027 ± .016	1.63 ± .24	300 ± 30
2.778 ± .011	1.20 ± .26	230 ± 40
2.54	0.40	----
2.321 ± .006	1.99 ± .21	80 ± 20
2.138 ± .010	1.79 ± .22	140 ± 30
1.90	0.45	----
1.641 ± .006	0.76 ± .09	65 ± 25
0.735 ± .003	1.06 ± .06	45 ± 10
0.511 ± .001	36.5 ± .7	----

* The reported intensities are in units of ($10^{-3}/cm^2/s$) at the detector. Angular dependence of the atmospheric spectrum and detector reponse are not accounted for in this measurement. Reported intensities approximate the absolute disk average intensity.

Table 2: List of Reaction Gamma Rays from ^{14}N and ^{16}O

INTERVAL	Z	SYMBOL	A	ENERGY	GSTART	GSTOP	ZNOTE	LINES
0.7-0.8	5	B	10	717.	717.	0.	R	0.735
	7	N	14	727.	5833.	5106.	L	
0.800 - 1.500	6	C	14	808.	6901.	6093.	-	(NONE)
	5	B	12	953.	953.	0.	-	
	3	Li	8	975.	975.	0.	-	
	5	B	10	1023.	1740.	717.	R	
	6	C	14	1248.	7341.	6093.	-	
	5	B	10	1437.	2154.	717.	-	
1.5-1.8	8	O	15	1617.	6859.	5242.	-	1.64
	7	N	14	1632.	3945.	2313.	RL	
	5	B	12	1668.	2621.	953.	-	
	5	B	12	1674.	1674.	0.	-	
1.8-2.2	7	N	15	1884.	7155.	5271.	-	2.14
	6	C	11	1995.	1995.	0.	R	
	7	N	15	2000.	9155.	7155.	-	
	8	O	15	2034.	7276.	5242.	-	
	5	B	11	2124.	2124.	0.	RL	
	5	B	10	2154.	2154.	0.	-	
	8	O	16	2190.	11060.	8872.	L	
2.2-2.4	7	N	15	2295.	7566.	5271.	-	2.32
	5	B	11	2298.	6743.	4444.	-	
	7	N	14	2313.	2313.	0.	RL	
2.4-2.9	4	Be	10	2593.	5959.	3366.	-	2.78
	3	Li	9	2691.	2691.	0.	-	
	5	B	12	2723.	2723.	0.	-	
	8	O	16	2741.	8872.	6131.	RL	
	5	B	10	2867.	3585.	717.	-	
	4	Be	10	2896.	6262.	3366.	-	
2.9-3.2	6	C	13	3086.	3086.	0.	L	3.03
3.2-3.5	7	N	15	3305.	8576.	5271.	-	3.40
	6	C	10	3359.	3360.	0.	-	
	4	Be	10	3365.	3366.	0.	-	
	7	N	14	3378.	5691.	2313.	L	
	5	B	13	3483.	3483.	0.	-	
3.5-3.8	5	B	13	3534.	3535.	0.	-	3.69
	3	Li	6	3561.	3562.	0.	-	
	6	C	13	3684.	3684.	0.	RL	
	5	B	13	3711.	3712.	0.	-	

3.8-4.0	6 C	13	3853.	3854.	0.	RL	3.91
	7 N	14	3884.	6198.	2313.	L	
4.0-4.3	5 B	13	4131.	4132.	0.	-	4.19
	8 O	16	4140.	11060.	6919.	L	
4.3-4.6	6 C	11	4304.	4305.	0.	-	4.45
	6 C	11	4343.	6339.	1995.	-	
	6 C	12	4438.	4439.	0.	RL	
	5 B	11	4443.	4444.	0.	RL	
4.6-5.4	5 B	11	4667.	6793.	2124.	-	5.11
	6 C	11	4793.	4794.	0.	-	
	7 N	14	4912.	4913.	0.	L	
	5 B	11	5018.	5019.	0.	-	
	7 N	14	5105.	5106.	0.	RL	
	8 O	15	5180.	5181.	0.	R	
	8 O	15	5240.	5242.	0.	R	
	7 N	15	5270.	5271.	0.	RL	
	[illegible]	[illegible]	5298.	[illegible]	0.	R	
5.4-5.9	6 C	11	5513.	7509.	1995.	-	5.61
	7 N	14	5690.	5691.	0.	L	5.85
	7 N	14	5832.	5833.	0.	L	
	5 B	11	5870.	7996.	2124.	-	
5.9-6.3	4 Be	10	5958.	5960.	0.	-	6.18
	6 C	14	6092.	6093.	0.	L	
	8 O	16	6129.	6131.	0.	RL	
	8 O	15	6176.	6177.	0.	R	
	7 N	14	6196.	6198.	0.	-	
6.3-6.6	7 N	15	6322.	6324.	0.	RL	6.46
	6 C	11	6337.	6339.	0.	R	
	5 B	11	6440.	8566.	2124.	-	
	7 N	14	6442.	6444.	0.	L	
	6 C	11	6478.	6480.	0.	R	
6.6-7.2	6 C	14	6726.	6728.	0.	L	6.93
	5 B	11	6741.	6743.	0.	R	
	8 O	15	6786.	6788.	0.	-	
	5 B	11	6791.	6793.	0.	R	
	6 C	11	6904.	6906.	0.	-	
	8 O	16	6917.	6919.	0.	RL	
	6 C	14	7010.	7012.	0.	-	
	7 N	14	7026.	7028.	0.	L	
	8 O	16	7117.	7119.	0.	RL	
7.2-8.5	5 B	11	7293.	7296.	0.	-	(NONE)
	7 N	15	7299.	7301.	0.	RL	
	6 C	11	7506.	7509.	0.	-	

[illegible]	1	7993.	7996.	0. -
	5	8310.	8313.	0. -

Notes on final typing of tables.

The order of the rows in Table 1 should be reversed, that is, the row starting with 0.511 MeV should be first and the row beginning with 6.927 MeV should be last.

Table 2 should be restructured as follows.

Table 2: Comparison of Observed Line Feature Energies with Reaction Gamma Ray Lines from ^{14}N and ^{16}O

Energy Interval*	Reaction Line Energy	Nuclide and Transition Level Energies	Note**	Observed Features
0.7 - 0.8	0.717	^{10}B (0.717-g.s.)	R	0.735
	0.727	^{14}N (5.833-5.106)	L	
0.8 - 1.5	0.808	^{14}C (6.901-6.093)	-	(none)
	0.953	^{12}B (0.953-g.s.)	-	

.
.
.
.

* All *energies in* MeV

** L = Neutron-induced line compiled by Ling (1975)
R = Proton-induced line compiled by Ramaty et al. (1979)
- = Not used in previous astrophysical studies of the Moon, Earth's atmosphere, and solar flares.

FIGURE CAPTIONS

1. Raw atmospheric gamma-ray count spectrum. A 48 day sum of counts from the Gamma Ray Spectrometer obtained while the instrument was pointing downward, toward the atmosphere. Some strong background lines intrinsic to the detector are indicated.

2. The atmospheric gamma-ray count spectrum obtained by normalized subtraction of an upward pointing spectrum from the atmospheric specrum. There are no visible residual detector background lines. Atmospheric line intensities are enhanced by restricting the time of collection to periods where the vertical rigidity cutoff is low (< 11 MeV).

3. The 0.511 MeV line from the atmosphere fit with and without atmospheric Compton scattering. Model photon spectra are compared with the observed count spectrum using the detector model.

4. Count spectrum between 0.8 MeV and 2.0 MeV with model fit superimposed.

5. Count spectrum between 2.0 MeV and 4.0 MeV with model fit superimposed.

6. Count spectrum between 4.0 MeV and 6.0 MeV with model fit superimposed.

7. Count spectrum between 6.0 MeV and 8.0 MeV with model fit superimposed.

8. Comparison of observed atmospheric gamma-ray line feature intensities with predictions of Ling (1975) and calculated intensities based on Reedy's (1978) lunar intensities.

This page intentionally left blank.
Figure 1 to be provided by the Naval
Research Laboratory.

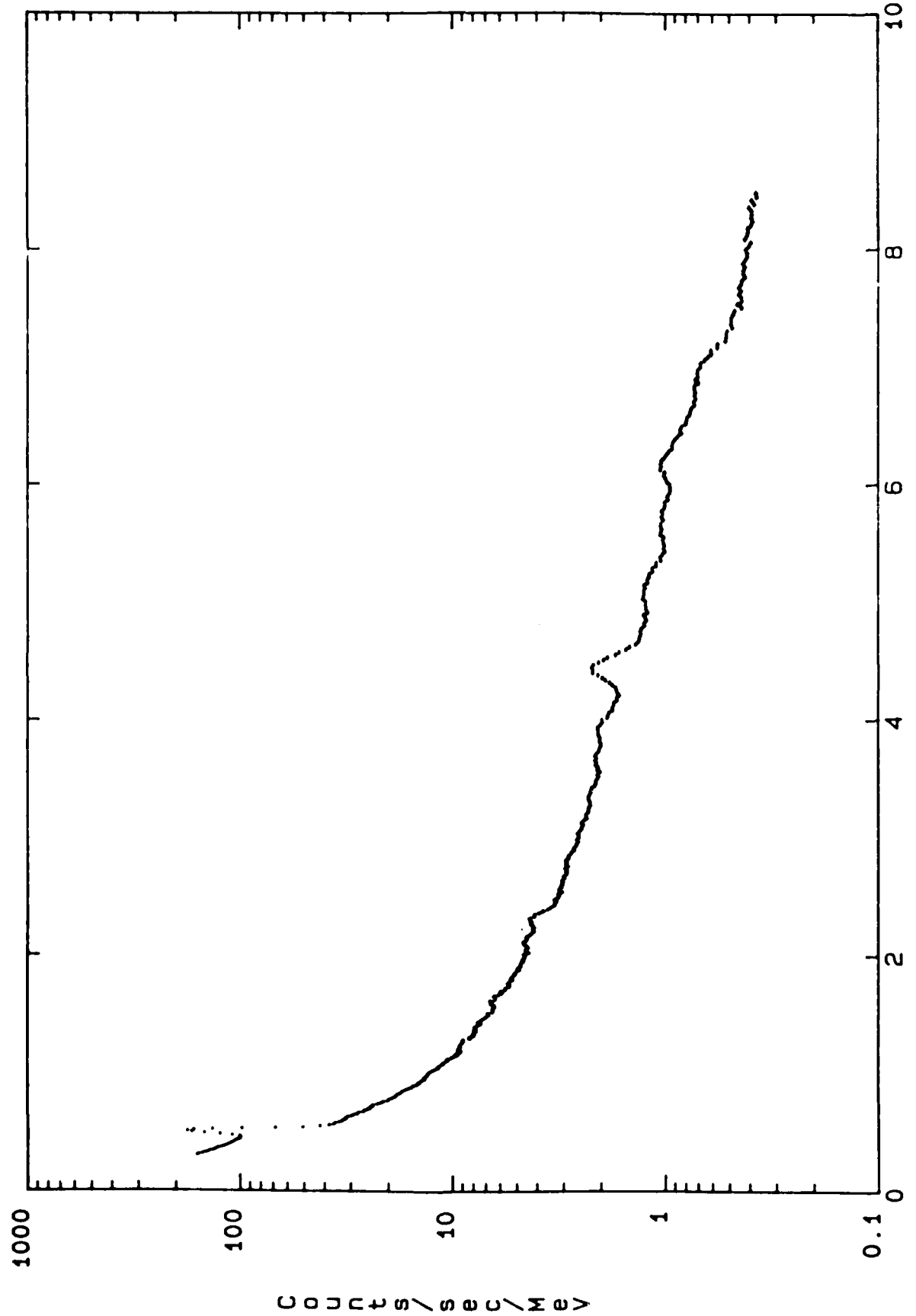

Figure 2

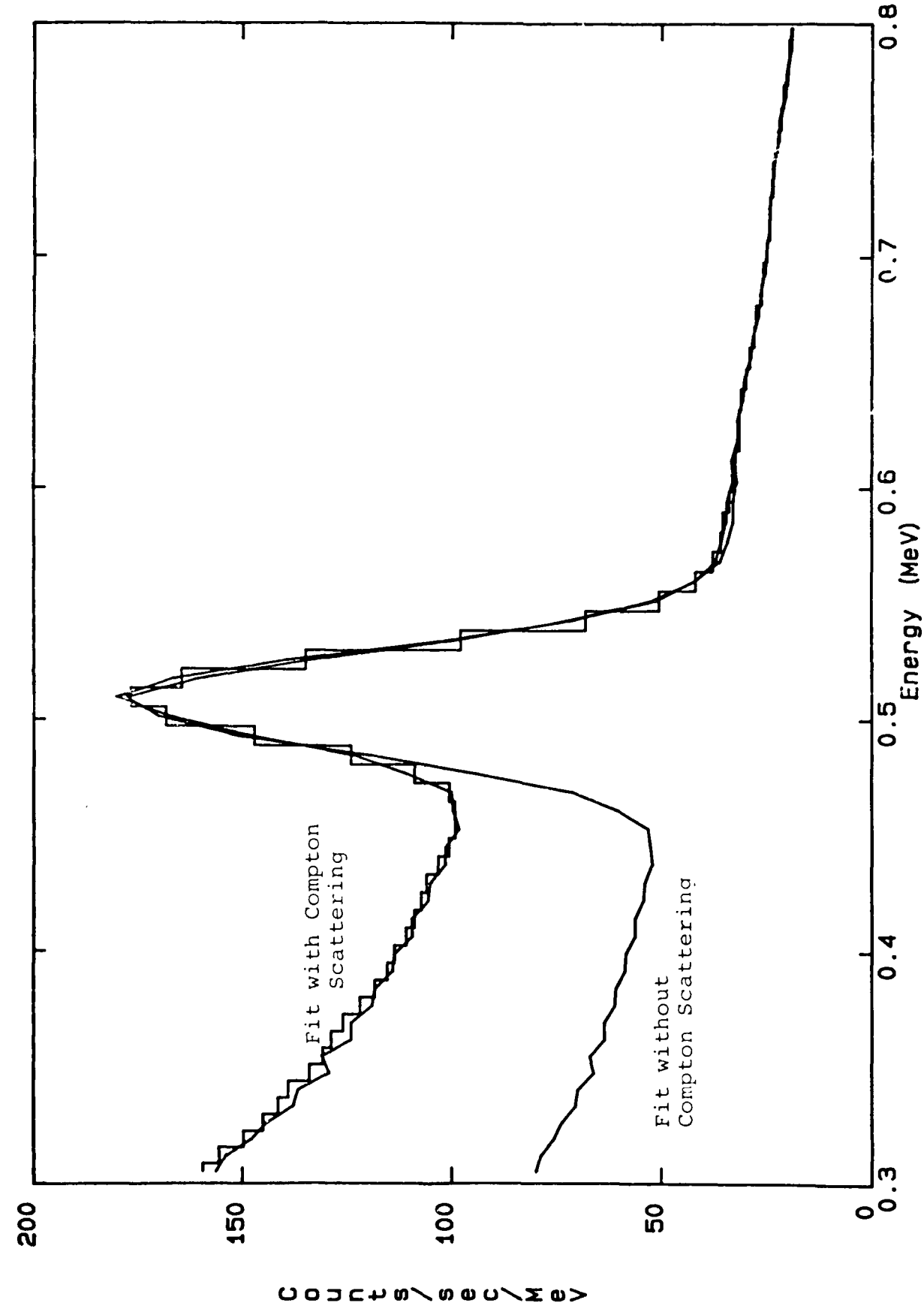
Counts/sec/MeV
200
150
100
50
0
0.3
0.4
0.5
0.6
0.7
0.8
Energy (MeV)
Fit with Compton Scattering
Fit without Compton Scattering

Figure 3

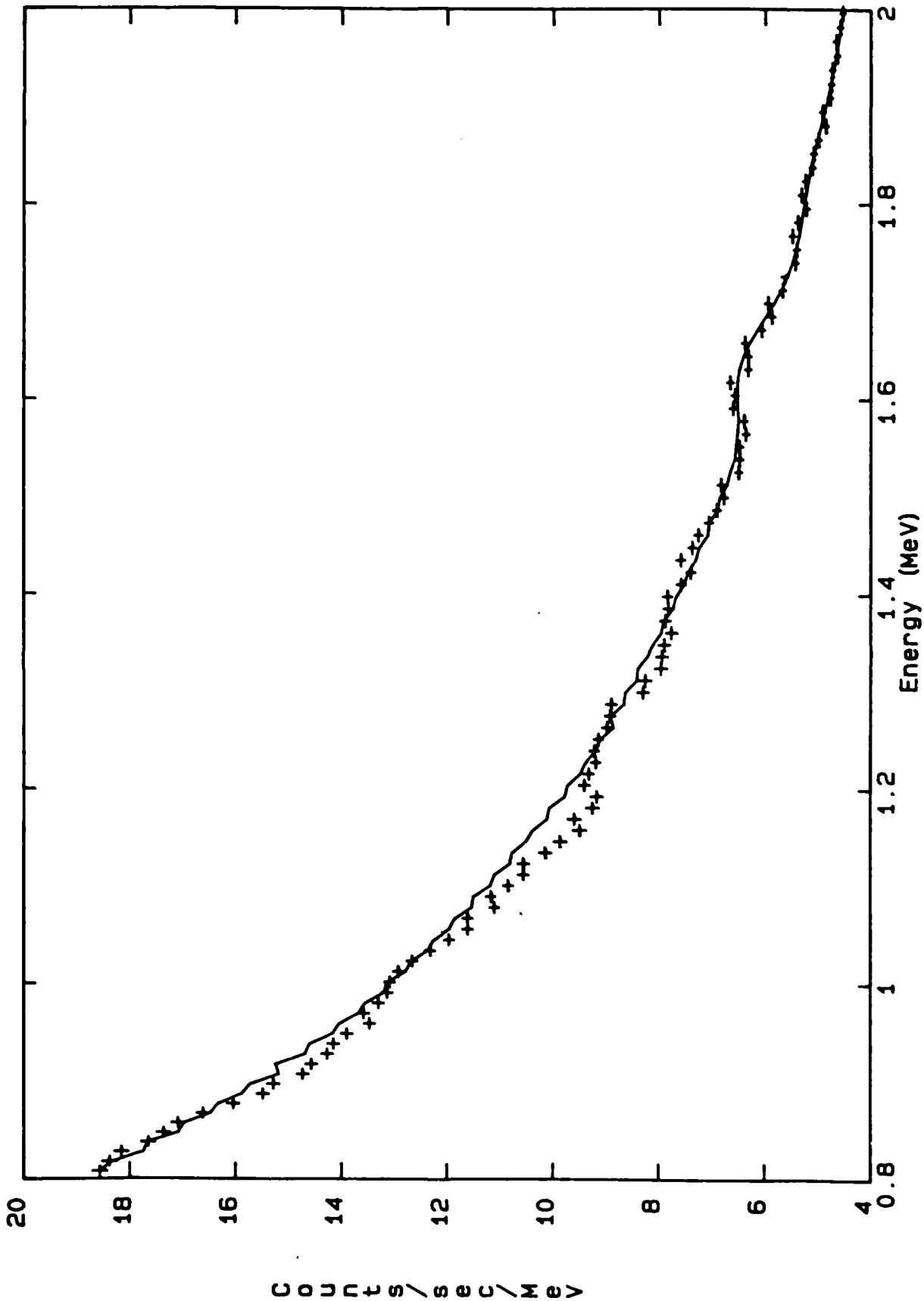

Figure 4

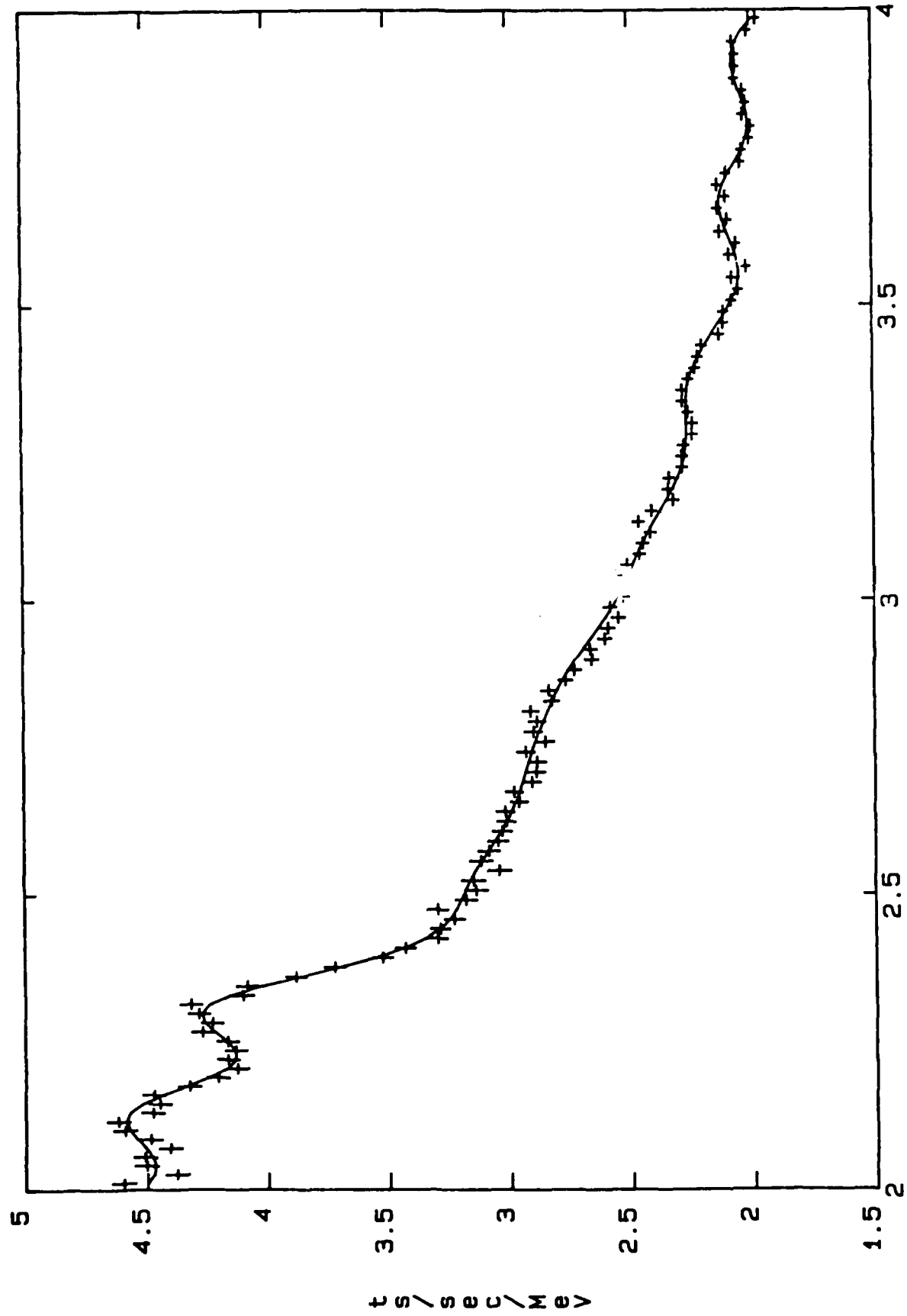

Figure 5

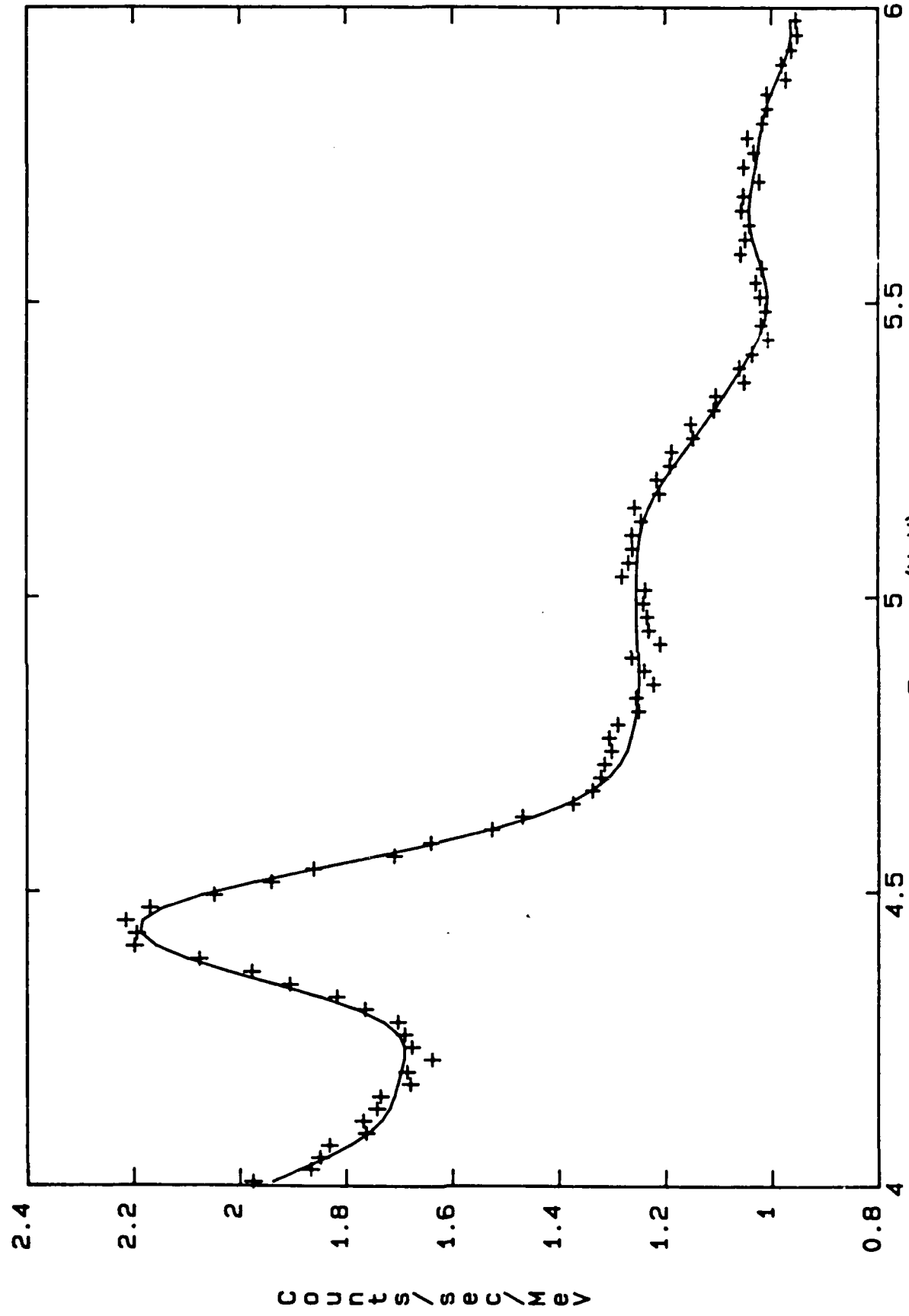

Figure 6

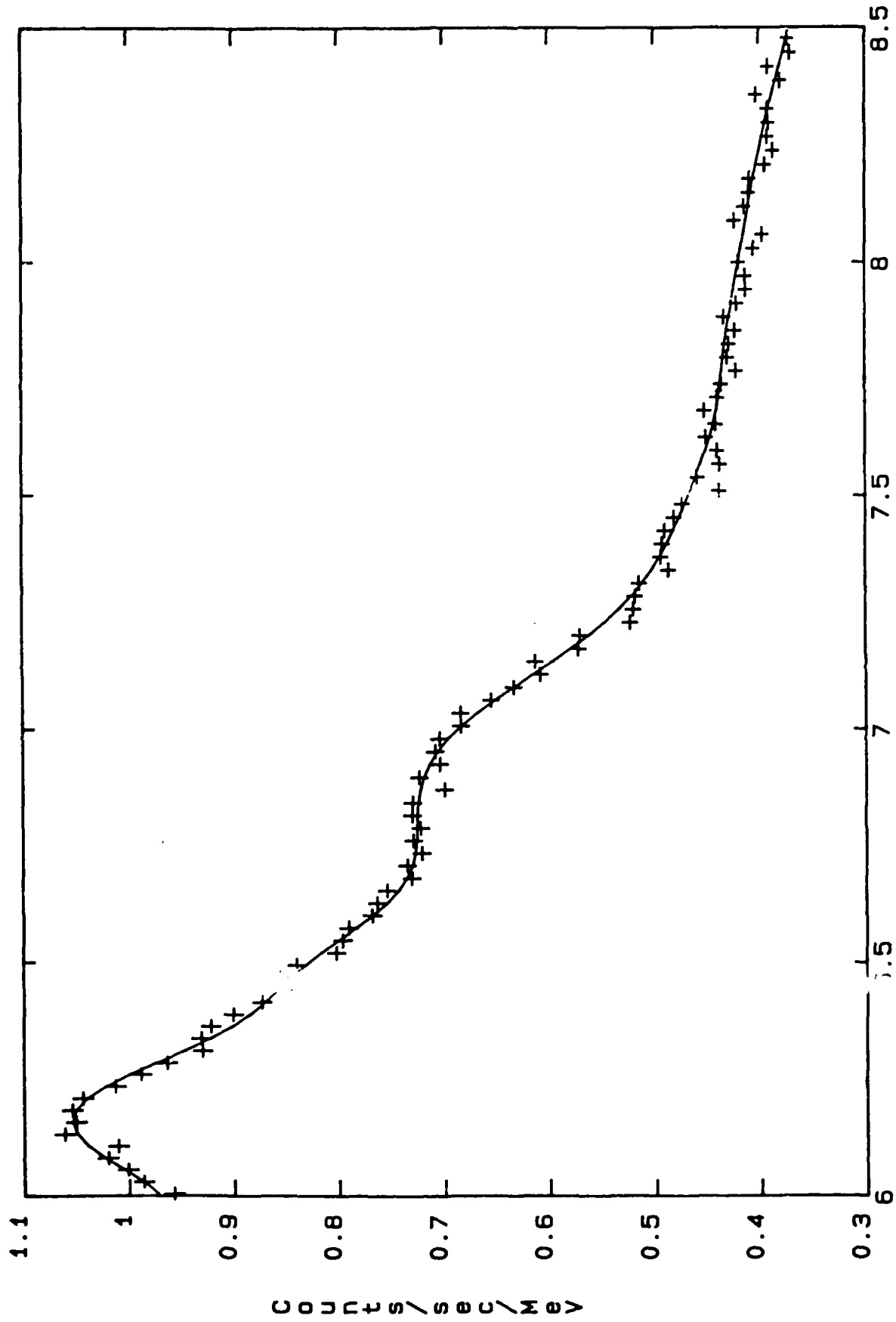

Figure 7

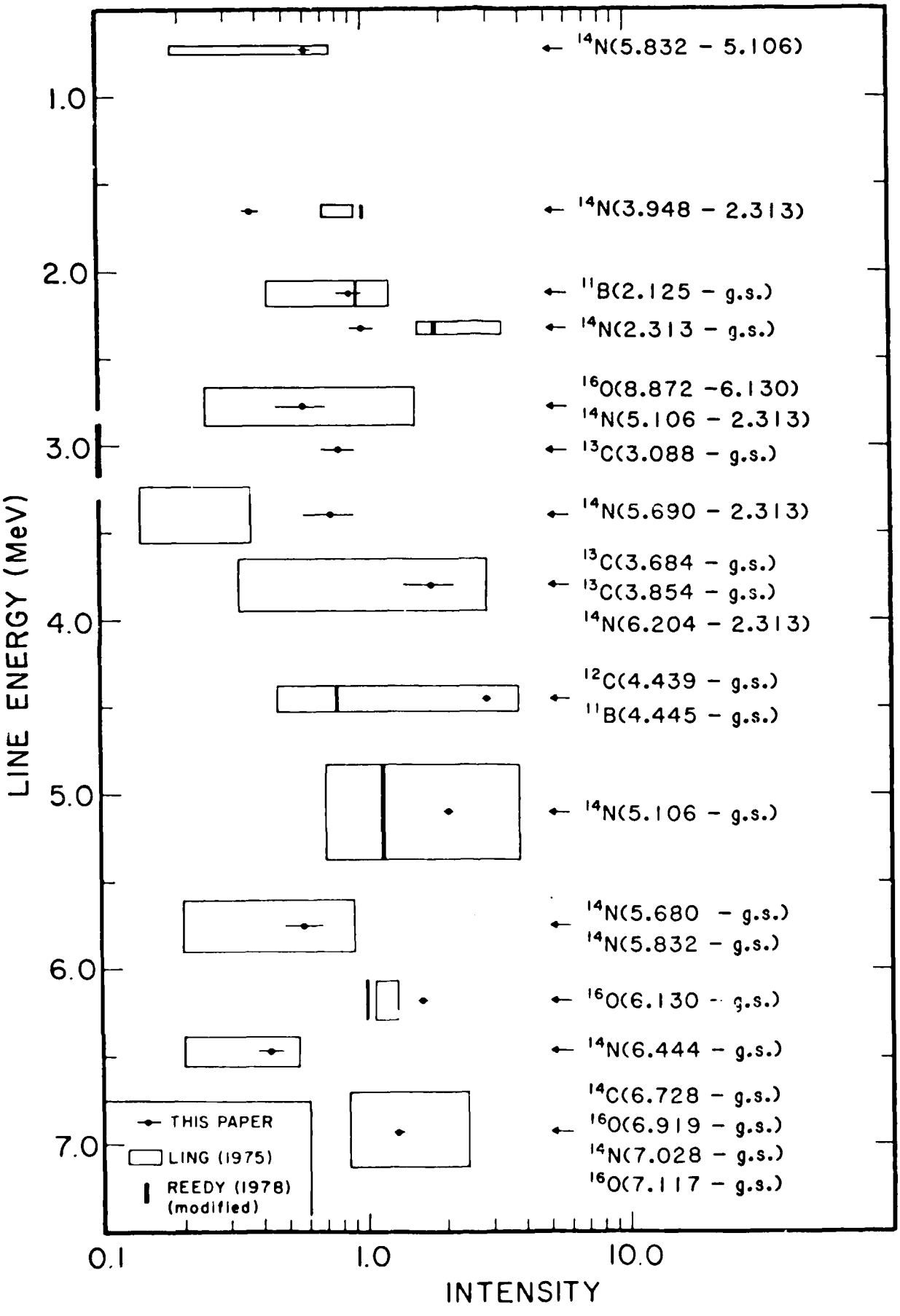
LINE ENERGY (MeV)
1.0
2.0
3.0
4.0
5.0
6.0
7.0
0.1
1.0
10.0
INTENSITY
(relative to mean of 1.632 and 6.129 MeV lines)
← 14N(5.832 - 5.106)
← 14N(3.948 - 2.313)
← 11B(2.125 - g.s.)
← 14N(2.313 - g.s.)
← 16O(8.872 -6.130)
← 14N(5.106 - 2.313)
← 13C(3.088 - g.s.)
← 14N(5.690 - 2.313)
← 13C(3.684 - g.s.)
← 13C(3.854 - g.s.)
14N(6.204 - 2.313)
← 12C(4.439 - g.s.)
11B(4.445 - g.s.)
← 14N(5.106 - g.s.)
← 14N(5.680 - g.s.)
14N(5.832 - g.s.)
← 16O(6.130 - g.s.)
← 14N(6.444 - g.s.)
14C(6.728 - g.s.)
← 16O(6.919 - g.s.)
14N(7.028 - g.s.)
16O(7.117 - g.s.)
THIS PAPER
LING (1975)
REEDY (1978)
(modified)

Figure 8

END

4-87

DTIC